HHS Public Access

Author manuscript

Mol Cancer Ther. Author manuscript; available in PMC 2017 May 01.

Published in final edited form as:

Mol Cancer Ther. 2016 May ; 15(5): 1113–1122. doi:10.1158/1535-7163.MCT-15-0769.

MR Studies of Glioblastoma Models Treated with Dual PI3K/mTOR Inhibitor and Temozolomide – Metabolic Changes are Associated with Enhanced Survival

Marina Radoul[1], **Myriam M. Chaumeil**[1], **Pia Eriksson**[1], **Alan S. Wang**[1], **Joanna J. Phillips**[2], and **Sabrina M. Ronen**[1]

[1]Department of Radiology and Biomedical Imaging, University of California San Francisco, San Francisco, CA 94143

[2]Brain Tumor Research Center, University of California San Francisco, San Francisco, CA 94143

Abstract

Current standard of care for glioblastoma (GBM) is surgical resection, radiation, and treatment with Temozolomide (TMZ). However, resistance to current therapies and recurrence are common. To improve survival, agents that target the phosphoinositide-3-kinase (PI3K) signaling pathway, which is activated in ∼88% of GBM, are currently in clinical trials. A challenge with such therapies is that tumor shrinkage is not always observed. New imaging methods are therefore needed to monitor response to therapy and predict survival. The goal of this study was to determine whether hyperpolarized ^{13}C magnetic resonance spectroscopic imaging (MRSI) and ^{1}H magnetic resonance spectroscopy (MRS) can be used to monitor response to the second-generation dual PI3K/mTOR inhibitor voxtalisib (XL765, SAR245409), alone or in combination with TMZ. We investigated GS-2 and U87-MG GBM orthotopic tumors in mice, and used magnetic resonance imaging (MRI), hyperpolarized ^{13}C MRSI and ^{1}H MRS to monitor the effects of treatment. In our study, ^{1}H MRS could not predict tumor response to therapy. However, in both our models, we observed a significantly lower hyperpolarized lactate-to-pyruvate ratio in animals treated with voxtalisib, TMZ, or combination therapy, when compared to controls. This metabolic alteration was observed prior to MRI-detectable changes in tumor size, was consistent with drug-action, and was associated with enhanced animal survival. Our findings confirm the potential translational value of the hyperpolarized lactate-to-pyruvate ratio as a biomarker for noninvasively assessing the effects of emerging therapies for patients with GBM.

Keywords

Glioblastoma; PI3K/mTOR inhibitor; hyperpolarized ^{13}C MRSI

Corresponding Author: Sabrina M. Ronen, Ph.D., Box 2532 UCSF Mission Bay Campus, Byers Hall, Rm BH303E, 1700 4th Street, San Francisco, CA 94143, ; Email: sabrina.ronen@ucsf.edu, Phone: 415-514-4839, Fax: 415-514-2550.

Conflict of Interest: The authors declare no conflicts of interest.

Introduction

Glioblastoma (GBM) is one of the most aggressive and fatal types of malignant gliomawith a very poor prognosis regardless of how early the tumor is detected. According to the Central Brain Tumor Registry of the United States for 2006–2010, GBM accounts for more than 50% of all newly diagnosed glioma cases (1). Current standard of care for GBM is safe surgical resection, followed by radiotherapy and Temozolomide (TMZ) treatment (2, 3). However, diffuse infiltration of tumor cells into eloquent regions of the normal brain precludes full surgical resection. Additionally, development of resistance to radiotherapy and TMZ is common (4, 5), and the heterogeneous biology of GBM further complicates therapy (6). Thus, despite harsh anticancer treatments, GBM tumors always recur. Outcomes can vary with tumor size and location, but unfortunately average survival is still less than two years (1, 7). In light of this dismal prognosis, recent work has focused on the development of alternative and complementary treatment strategies.

Data from The Cancer Genome Atlas shows that ∼88% of GBM have activated the phosphoinositide-3-kinase (PI3K) pathway (8). This central signaling pathway is involved in essential cellular functions such as growth, migration, proliferation, metabolism and survival. The PI3K pathway can be activated at different steps of the signaling cascade, most notably by loss of the phosphatase and tensin homologue (PTEN) protein, and by amplification and/or mutation of the epidermal growth factor receptor (EGFR), which occur in 40% and 50% of GBM cases, respectively (8). Accordingly, several drugs that inhibit signaling downstream of these mutations are currently in phase I and II clinical trials, either in combination with other FDA-approved chemotherapeutic agents such TMZ, or as single agents (9–13). Importantly, whereas first generation PI3K pathway inhibitors target mostly the downstream node of mTOR, the observation of feedback loops that result in enhanced PI3K signaling has led to the development of second-generation drugs (14–17). These target both mTOR and PI3K and generally overcome the negative feedback (18, 19).

Current clinical evaluation of response to treatment for GBM is most commonly based on tumor size as detected by magnetic resonance imaging (MRI) (20). However, in the case of PI3K pathway inhibitors, treatment often induces tumor stasis rather than shrinkage, limiting the utility of anatomic imaging (21). Alternative imaging methods that can probe for drug-target engagement and assess response are therefore critically needed to improve timely clinical patient management.

One possible approach is the imaging of metabolism. The value of ^{1}H MR spectroscopy (MRS) in detecting the metabolic alterations characteristic of GBM has been clearly demonstrated in the clinic (22–24). Levels of MRS-detectable total choline-containing metabolites (tCho) are elevated in tumors when compared to normal brain, whereas levels of N-acetyl aspartate (NAA) are reduced. Interestingly, elevated tCho and phosphocholine (PC) levels have also been linked to activation of PI3K signaling, and inhibition of this signaling pathway has resulted in a drop in PC levels in several cancer types including GBM (25–28). Based on these previous findings, tCho levels could serve to assess response to PI3K pathway inhibitors.

An alternate approach for monitoring modulations of the PI3K pathway is the recently developed hyperpolarized ^{13}C MRSI approach. Hyperpolarization improves the signal-to-noise ratio for ^{13}C-labeled substrates by over 10,000-fold, and thus enables rapid non-invasive *in vivo* imaging of the metabolism of hyperpolarized substrates (29–31). Previous studies from our group have shown that the level of hyperpolarized [1-^{13}C]-lactate produced from exogenous hyperpolarized [1-^{13}C]-pyruvate decreases in several GBM cell lines following inhibition of the PI3K pathway either at the level of PI3K or at the level of mTOR. A drop in hyperpolarized [1-^{13}C]-lactate was also observed *in vivo* following mTOR inhibition in a rat GBM model (26, 32, 33). These metabolic observations were linked to drug-action via the decreased expression of lactate dehydrogenase (LDH-A), which is controlled by PI3K signaling and catalyzes the pyruvate-to-lactate conversion (32). ^{13}C MRSI was also used to probe the effect of TMZ on hyperpolarized [1-^{13}C]-lactate production. A drop in hyperpolarized [1-^{13}C]-lactate levels was shown to precede tumor shrinkage in GBM *in vivo*, mediated by a drop in intracellular lactate levels (34, 35). Importantly, the first-in-human clinical study using hyperpolarized [1-^{13}C]-pyruvate in prostate cancer patients showed no toxicity and was highly sensitive in detecting elevated hyperpolarized [1-^{13}C]-lactate levels in regions of cancer (36). The hyperpolarized ^{13}C MRSI approach could therefore also serve for clinical assessment of PI3K inhibitors, either alone or in combination with TMZ.

However, none of the previous MRS studies have investigated the impact in GBM of novel second-generation inhibitors that target *both* PI3K and mTOR, and that are now in clinical trials. Furthermore, no previous studies have determined whether changes in ^{1}H MRS and hyperpolarized ^{13}C MRSI are associated with increased survival following treatment. The goal of this study was therefore to use ^{1}H MRS and hyperpolarized ^{13}C MRSI to monitor the effect of a dual PI3K/mTOR inhibitor, either alone or in combination with TMZ, in two orthotopic brain tumor models. We focused on the dual PI3K/mTOR inhibitor, voxtalisib (SAR245409, XL765), which is a pan-class I PI3K, mTORC1 and mTORC2 inhibitor (15, 16), and investigated its impact on two GBM models that exhibit activated PI3K signaling via PTEN deletion, GS-2 and U87-MG, as orthotopic tumors in mice. Surprisingly, we found that tCho levels were not altered by treatment. In contrast, in both of our models, the hyperpolarized lactate-to-pyruvate ratio (Lac/Pyr) as detected by ^{13}C MRSI was significantly lower following treatment. The metabolic changes were associated with enhanced animal survival and generally preceded detectable change in tumor size following treatment with voxtalisib either alone or in combination with TMZ. Our findings highlight the value of hyperpolarized ^{13}C MRSI as a potentially translational method for noninvasive assessment of the effect of novel second-generation dual PI3K inhibitors.

Materials and Methods

Cell culture

GS-2 and U87-MG human GBM cells (26, 32) were supplied by the UCSF Brain Tumor Research Center Preclinical Therapeutics Core in 2009 and 2010 respectively. Cells were routinely fingerprinted by the UCSF Genomics Core Facility using single nucleotide polymorphism (last fingerprinting 08/28/14) and maintained in culture less than 6 months.

Cells were cultured in DMEM (GIBCO) supplemented with 10% FBS, 2mM L-glutamine, 100 units/ml penicillin and 100 μg/ml streptomycin in 5% CO_2 at 37°C.

Drugs

Voxtalisib, (SAR245409, XL765) was kindly provided by Sanofi (Exelixis). Voxtalisib was prepared by sonication in 10mM HCl. TMZ (Sigma-Aldrich) was dissolved in ORA-plus (Perrigo). All drugs were prepared right before administration.

Animal models and study design

All studies were performed under UCSF Institutional Animal Care and Use Committee approval. 6–7 week-old female athymic nu/nu mice (20–25g) were intracranially injected with ~3×10^5 GS-2 or U87-MG cells. Tumor size was evaluated using MRI. Once tumors reached 2–3 mm in diameter, a baseline set of MR studies was performed (see below). This time point was considered day zero (D0). Mice were then randomized into four treatment groups and treated per os (p.o.) with: (1) 30mg/kg voxtalisib twice daily; (2) 5mg/kg TMZ daily; (3) 30mg/kg voxtalisib twice daily and 5mg/kg TMZ daily (TMZ was given 1h after the first dose of voxtalisib); (4) 10mM HCl daily (for controls). MR studies were then repeated every 2–4 days and continued either until the animal had to be sacrificed or until the tumor was no longer detectable. At the end of the MR studies the brain was excised and divided into two halves. Half the tumor and contralateral normal-appearing brain were fixed in formalin for histological analysis. The second half was snap-frozen in liquid nitrogen and stored at −80°C until ^{1}H high-resolution magic angle spinning (HR-MAS) MR studies. To obtain tissue for histological and HR-MAS studies when treatments resulted in complete tumor shrinkage, additional studies were performed and animals were sacrificed when the tumor had shrunk to its original size at D0. In those cases, animal survival for the Kaplan-Meier survival curve was chosen as the time point at which tumor was no longer detectable.

In vivo MR studies

All studies were performed on a 14.1T vertical MR system (Agilent Technologies), equipped with single channel ^{1}H coil for T2-weighted imaging and ^{1}H MRS, or with dual-tune ^{1}H-^{13}C coil for hyperpolarized ^{13}C MRSI.

Anatomic MR Imaging

Axial T2-weighted images were used to evaluate tumor sizes and were recorded using a multi-slice spin-echo sequence with the following parameters: TE=20ms, TR=1200ms, FOV=30×30mm^2, matrix 256×256, slice thickness 1.8mm, NA=2. Tumor size was determined by manually contouring the tumor area in each axial slice and calculating the total volume as a sum of the areas multiplied by slice thickness using in-house MR software (37).

Hyperpolarized ^{13}C MR Spectroscopic imaging

[1-^{13}C]-pyruvic acid was prepared as previously (32) and 300μl injected intravenously through a tail-vein catheter over 12s. Spectra were then acquired as described below.

First, a preliminary dynamic study in a small number of untreated animals (n=3/model) was performed to determine the time course of hyperpolarized [1-^{13}C]-pyruvate delivery and maximum hyperpolarized [1-^{13}C]-lactate production. For this, a 2D chemical shift imaging (CSI) dynamic sequence was used over the course of 52.5s following hyperpolarized [1-^{13}C]-pyruvate injection with the following parameters: TE=1.2ms, TR=60ms, FA=10, matrix 128×7×7, spectral width 2500Hz, FOV=30×30mm^2, 4mm slice thickness, scan time 3.5s per time point, 15 time points. Data were then processed and peak integrals of hyperpolarized [1-^{13}C]-pyruvate and hyperpolarized [1-^{13}C]-lactate were quantified within the tumor voxel and a normal brain voxel using the SIVIC software (38). Hyperpolarized [1-^{13}C]-lactate integrals were normalized to noise and to maximum hyperpolarized [1-^{13}C]-pyruvate signal. The average time points at which hyperpolarized [1-^{13}C]-lactate was maximal in normal brain and in tumor voxels were then determined (∼17s for both tumor and normal brain in both models; see Results). Subsequent data was therefore recorded using a 2D–CSI pulse sequence at ∼17s post-injection of hyperpolarized [1-^{13}C]-pyruvate using: TE=0.41ms, TR=66 ms, FA=10, matrix 256×16x16, spectral width 4223Hz, FOV=20×20mm^2, 4 mm slice thickness. Data were processed using SIVIC (38). A tumor voxel was chosen after evaluation of all slices such that it contained >80% of tumor tissue, avoiding necrotic and inhomogeneous regions. Peak integrals corresponding to hyperpolarized [1-^{13}C]-pyruvate and [1-^{13}C]-lactate in the tumor voxel were used to calculate $\mathrm{Lac/Pyr}_{\mathrm{Di}}^{\mathrm{Tumor}}$, where *Di* is day of treatment (*i*=0,1…n) and further normalized to $\mathrm{Pyr}_{\mathrm{Di}}^{\mathrm{Contralateral}}$ obtained from contralateral brain such that:

$$\mathrm{Lac/Pyr}_{\mathrm{Di}}=\frac{\mathrm{Lac/Pyr}_{\mathrm{Di}}^{\mathrm{Tumor}}}{\mathrm{Lac/Pyr}_{\mathrm{Di}}^{\mathrm{Contralateral}}}$$

^{1}H MR spectroscopy

^{1}H MRS spectra were acquired from a 2×2×4 mm^3 voxel placed in the center of the tumor using a PRESS sequence with: TE=20ms, TR=4000ms, NA=256–512, 4096 points, spectral width 10000Hz. Spectra were analyzed using QUEST in jMRUI using a basis set with alanine (Ala), choline (Cho), phosphocholine (PC), glycerophosphocholine (GPC), creatine (Cr), phosphocreatine (PCr), glutamate (Glu), glutamine (Gln), glutathione (GSH), glycine (Gly), lactate (Lac), myo-inositol (mI), N-acetyl aspartate (NAA), and taurine (Tau) (39). Because Glu and Gln, Cr and PCr, and Lac and lipids overlap these metabolites were quantified as Glx, Cr and Lac+Lipids respectively. The integral of total choline (sum of Cho, PC and GPC) on *Di* was determined and normalized to the total signal $(tSignal)_{Di}$:

$$(\mathrm{tCho})_{\mathrm{Di}}^{\mathrm{Normalized}}=\frac{(\mathrm{tCho})_{\mathrm{Di}}}{(\mathrm{tSignal})_{\mathrm{Di}}}$$

^{1}H HR-MAS spectroscopy

Tissue samples were weighed and 17±5mg placed into a zirconia rotor, where 6μl of D_2O with 0.75 w/% 2,2,3,3-D4-3-(trimethylsilyl)propionic acid were added as chemical shift reference. All spectra were acquired on Agilent 500MHz spectrometer at 1°C. Samples were

spun at 2250Hz and Carr-Purcell-Meiboom-Gill sequence used with: TE=144 ms (train of 162 180° hard pulses 0.888μs apart) and 512 transients. Spectra were analyzed using MestReNova (MestreLab Research) and peak integrals were normalized to total signal (40).

Immunohistochemistry

After the MR study, tissues were fixed in formalin for 24h then dehydrated with ethanol and embedded in paraplast Plus wax (McCormick Scientific). Tumor tissue sections were probed with antibodies for: lactate dehydrogenase (LDH)-A (Cell Signaling), carbonic anhydrase IX (CAIX; Novus Biologicals), phospho-S6 ribosomal protein (Ser240/244; Cell Signaling) and phospho-Chk1 (Ser345, Cell Signaling) to inform on LDH-A expression, HIF-1 expression, PI3K signaling, and TMZ action respectively. The stained slides were imaged using Nikon Eclipse Ti-E motorized inverted microscope.

Statistical analysis

Results represent mean ± standard deviation. Two-tailed unpaired Student's t-test was used to determine the statistical significance of differences, and *P*-value ≤ 0.05 was considered significant. Kaplan-Meier survival curves with Log-rank test were used to compare survival.

Results

Preliminary optimization and validation studies

Previous hyperpolarized studies to monitor response to therapy were performed on a 3T clinical scanner in rats and probed the effect of the mTOR inhibitor Everolimus in GS-2 tumors and the effect of TMZ in U87-MG tumors (32, 34, 35). We therefore first wanted to perform a small-scale study in which we optimized our data acquisition conditions for mice studies at 14.1T.

Tumors were detected using T2-weighted anatomical MRI (Fig. 1A and 1B). We then used a ^{13}C dynamic 2D–CSI sequence to assess the kinetics of hyperpolarized [1-^{13}C]-pyruvate delivery and hyperpolarized [1-^{13}C]-lactate production in GS-2 and U87-MG tumors as well as in normal brain. Our findings for lactate build-up and decay are illustrated in Figures 1C and D. We determined that maximum hyperpolarized [1-^{13}C]-lactate production was reached at 17.5±0s in normal brain and 17.5±3.5s in tumor in the GS-2 model (n=3), and at 17.5±0s in normal brain and 17.5±4.0s in tumor in the U87-MG model (n=3). Based on these finding, we performed our subsequent investigations using a 2D–CSI sequence at the single time point of maximum hyperpolarized [1-^{13}C]-lactate production (∼17s) in order to achieve the best possible sensitivity and spatial resolution.

Next, we wanted to confirm that previous findings in rats with regard to the effect of treatment on lactate production (32, 34, 35) also hold in mice. We therefore treated GS-2-bearing mice (n=5) with Everolimus, and U87-MG-bearing animals (n=4) with TMZ, and compared our findings to control tumors (n=5 for each tumor model). We confirmed that treatment of GS-2 tumors with Everolimus for 9±2 days (Fig. 1E) and treatment of U87-MG tumors with TMZ for 6±1 days (Fig. 1F) resulted in a significantly lower level of hyperpolarized Lac/Pyr when compared to controls (P<0.05 for CTRL vs. Everolimus in

GS-2 tumors, $P<0.03$ for CTRL vs. TMZ in U87-MG tumors). These findings recapitulated the previous observations in rats on a 3T clinical scanner, and paved the way for our studies monitoring the dual PI3K/mTOR inhibitor in mice at 14.1T (32, 34, 35).

Effect of treatment in the GS-2 model

In vivo hyperpolarized ^{13}C MRSI—The GS-2 xenografts reached a size of 0.1±0.01cm^3, sufficient for hyperpolarized ^{13}C MRSI studies, at 38±9 days post-implantation. Figure 2A exhibits axial T2-weighted images and hyperpolarized ^{13}C MRSI spectra from tumor voxels from each treatment group recorded at D0, prior to treatment, and at D9±2 of treatment. Average data illustrating the temporal evolution of tumor sizes in the different treatment groups is shown in Figure 2B. Whereas administration of voxtalisib (n=5) did not significantly affect tumor growth, administration of combination voxtalisib/TMZ (n=5) and TMZ alone (n=6) led to tumor shrinkage that was significant by D14 of treatment ($P<0.05$) when compared to control animals (n=5). Next, we focused on the time interval of D9±2, prior to any significant change in tumor size when comparing treated animals to controls (Fig. 2C). As illustrated in Figure 2D, treatment led to a significantly lower level of hyperpolarized Lac/Pyr at this time point for every treatment group when compared to controls ($P\leq0.05$ for all treatments). Kaplan-Meier survival curves (Fig. 2E) demonstrate the significantly improved survival of mice treated with voxtalisib (n=5, Log-rank $P<0.001$), voxtalisib/TMZ combination (n=5, Log-rank $P<0.001$) or TMZ (n=6, Log-rank $P<0.001$) compared to the controls (n=5). Lower hyperpolarized Lac/Pyr detected in treated tumors at D9±2 was therefore associated with improved survival, whereas tumor size was unchanged at this time, and could not inform on response.

Immunohistochemistry—Previous studies have shown that following treatment with PI3K pathway inhibitors, lower hyperpolarized lactate production is mediated by a reduction in the level of HIF-1, which leads to a reduction in the expression of LDH-A, the enzyme that catalyzes the pyruvate-to-lactate conversion (32, 33, 41). It has also been shown that following TMZ-treatment lower hyperpolarized lactate production is mediated by an increase in phospho-Chk1 levels, which leads to a drop in intracellular lactate levels and thus hyperpolarized lactate production (34, 35). In order to confirm that our observations were mechanistically linked to PI3K pathway inhibition and to TMZ action in a similar manner, we performed immunohistochemical (IHC) analyses on our tumors resected at the end of the MR studies (Fig. 3). The expression of CA-IX is controlled by HIF-1, and therefore staining for CA-IX informed on HIF-1 levels. Our findings show a drop in CA-IX, as well as a drop in LDH-A expression, following voxtalisib treatment, either alone or with TMZ. Staining for phospho-S6, which is downstream of PI3K and mTOR, also dropped following voxtalisib exposure, confirming inhibition of signaling via the PI3K pathway. Following treatment with TMZ, either alone or in combination with voxtalisib, an increase in phospho-Chk1 was observed. Our findings are thus consistent with previous work, linking drug action to the metabolic alterations observed by MRS in GS-2 tumors.

^{1}H MR Spectroscopy—We also wanted to determine whether tCho can serve as a biomarker for tumor response to therapy with the dual PI3K/mTOR inhibitor, as previously observed *in vivo* with the PI3K inhibitor PX-866, and in cells with the PI3K inhibitor

LY294002 (26, 28). We therefore acquired ^{1}H MR spectra from the tumor voxel. Figure 4A exhibits axial T2-weighed images of mice from the different treatment groups and their corresponding tumor spectra acquired on D9±2 of treatment. Figure 4B illustrates the average levels of tCho. Unexpectedly, tCho levels did not exhibit a significant change as a result of treatment with voxtalisib (n=4, P=0.34). However, treatment with combination voxtalisib/TMZ (n=3, P=0.06) showed a trend towards a decrease, and treatment with TMZ alone resulted in a significantly lower level of tCho by 33% (n=3, P<0.05) compared to controls (n=5). No changes were detected in any other metabolites in the ^{1}H MRS spectrum nor in metabolite ratios, including Ala, Cr, GSH, NAA, m-Ins, Tau, Gly, Glx, Lac+Lipid, NAA/Cr and Cho/Cr (Supplementary Table S1).

To confirm our *in vivo* findings, we also analyzed frozen resected tumor samples using ^{1}H HR-MAS, a method that provides higher spectral resolution and thus improved metabolite quantification. Figure 4C shows the effect of treatment on choline-containing metabolites. The HR-MAS data (Fig. 4D) confirmed the *in vivo* findings for all treatment groups. Levels of tCho did not change significantly as a result of treatment with either voxtalisib (n=4, P=0.59) or combination voxtalisib/TMZ (n=4, P=0.64) when compared to controls (n=4) but in the case of treatment with TMZ tCho was significantly lower by 31% (n=4, P<0.05). When considering the metabolites that comprise the tCho peak, no significant changes could be detected in any individual metabolite following any of the treatments. Furthermore, consistent with our *in vivo* findings no other metabolites or metabolite ratios changed with treatment (Supplementary Table S2).

Effect of treatment in the U87-MG model

To further confirm our findings, we also investigated a second GBM model, the U87-MG. Despite the same number of injected cells, U87-MG tumors grew faster than GS-2 and reached a size of 0.09±0.03 cm^{3}, sufficient for MRS studies, by 18±3 days post-implantation. We then performed similar MRS studies to those described above for the GS-2 model.

In vivo hyperpolarized ^{13}C MRSI—Axial T2-weighted images of mice from each group of treatment are shown in Figure 5A. Images and corresponding hyperpolarized ^{13}C MRSI spectra were recorded at D0, prior to onset of treatment and at D6±1 of treatment. Figure 5B illustrates the temporal evolution of tumor size and shows that treatment with voxtalisib (n=5) led to a rapid slowdown of tumor growth that was significant compared to controls (n=5, P<0.05) by D5±1. Treatment with TMZ (n=4) and combination voxtalisib/TMZ (n=5) resulted in a slowdown of tumor growth that was significant by D8±1 of treatment and was followed by frank tumor shrinkage that began around D12±1 of treatment. Focusing on D6±1, Figure 5C illustrates average tumor size. At this time point, a significant decrease in tumor size was detected as a result of treatment with voxtalisib, while changes in tumor size in the groups treated with combination voxtalisib/TMZ or TMZ were not yet significant compared to controls. However, hyperpolarized Lac/Pyr (Fig. 5D) was lower at D6±1 in all treatment groups when compared to controls (P<0.05 for all treatments). Average survival is illustrated using the Kaplan-Meier survival curves (Fig. 5E) and shows a significant increase in animal survival (Log-rank P<0.001) in all treatment groups. As in the case of the GS-2

model, the early change in hyperpolarized Lac/Pyr observed at D6±1 of treatment was associated with enhanced rodent survival in the U87-MG model.

^{1}H HR-MAS MR Spectroscopy—Our first tumor model (GS-2) only showed limited changes in tCho or any other metabolite. We therefore restricted our investigation of the U87-MG model to the higher resolution *ex vivo* ^{1}H HR-MAS studies. Figure 6A illustrates the ^{1}H HR-MAS data and the effect of treatment on choline-containing metabolites. Average tCho levels (Fig. 6B) show very comparable values among all treatment groups with no significant differences when compared to controls (n=3 for all treatment group, P=0.63 for voxtalisib, P=0.52 for voxtalisib/TMZ and P=0.51 for TMZ). When considering the metabolites that comprise the tCho peak, no significant changes could be detected in any metabolite and none of the other ^{1}H MRS-detectable metabolites or metabolite ratios changed with treatment in the U87-MG model (Supplementary Table S3).

Discussion

The vast majority of GBM tumors have activated their PI3K signaling pathway (8). PI3K inhibitors are therefore in clinical trials for treatment of GBM, either alone or in combination with the standard-of-care DNA damaging agent TMZ (34, 35). However, monitoring response to such therapies can be challenging because tumor shrinkage is not always observed (21). The goal of this study was therefore to expand upon our previous cell and *in vivo* studies (26, 32, 33, 35) and determine the clinical relevance of ^{1}H MRS-detectable choline-containing metabolite levels and ^{13}C MRSI-detectable hyperpolarized lactate-to-pyruvate ratio, as early biomarkers of drug-target engagement and possible indicators of enhanced survival following treatment with a previously unexplored second-generation dual PI3K/mTOR inhibitor in GBM.

We studied two orthotopic human GBM model, GS-2 and U87-MG, in mice. Both of these models are PTEN deficient and, as such, both have an activated PI3K signaling pathway and model the majority of GBM tumors. Tumors in the mouse brain cannot grow to a size that allows for more than one voxel to be placed within the tumor region without substantial partial volume effects from the surrounding normal parenchyma. As a result, any heterogeneity in tumor response could not be detected in our studies. Another possible limitation of our study is that it was performed using a 2D CSI sequence at the time point of maximum lactate production common to both tumor and normal brain. This allowed for better signal-to-noise compared to dynamic data. However, we cannot rule out that the time point for maximum lactate differs during treatment from the value observed in both tumor and normal brain. Nonetheless, we were able to confirm in mice previous observations in rats showing a drop in hyperpolarized lactate production following Everolimus and TMZ treatment (32, 35). Our findings are thus likely not species dependent.

Our studies were designed to mimic the clinic by investigating not only the dual PI3K/mTOR inhibitor, but also combination treatment with the standard of care TMZ. Furthermore, our studies used clinically-relevant dosing regimens and oral administration (16, 42). Interestingly, response to voxtalisib was quite different in both of our models. The U87-MG model responded by tumor shrinkage. In contrast the size of GS-2 tumors

remained indistinguishable from controls. A previous study in GBM39, showed that voxtalisib, either alone or in combination with TMZ, leads to a reduction in tumor size as measured by bioluminescence (43). The reasons for such differential effects on tumor growth remain to be determined. Nonetheless, in both of our models, the MRS observations were similar and were associated with enhanced survival.

Our previous work had shown that treatment with inhibitors of the PI3K pathway at the level of PI3K or mTOR alone resulted in ^{1}H and ^{31}P MRS detectable changes in tCho and PC both in cells and *in vivo*, in GBM and other cancers (26, 28). Surprisingly however, in both of our models, our findings did not indicate a significant change in tCho as a result of treatment with the dual PI3K/mTOR inhibitor. Previous reports investigating the effects of BEZ235 and PI-103, two other dual PI3K/mTOR inhibitors, showed either a drop or an increase in choline-containing metabolites (44–46). Further studies are therefore required to understand these discrepancies, which are likely associated with the complexity of the signaling pathways that control choline metabolism (25). Nonetheless our findings point to the challenges of using choline-metabolites as general biomarkers of response to inhibitors of the PI3K pathway.

In contrast, in both our models, lower levels of hyperpolarized Lac/Pyr were observed following drug exposure in every treatment group. We cannot rule out that the change in hyperpolarized pyruvate metabolism is a non-specific effect associated with response to therapy; similar metabolic effects have been reported with starvation-induced autophagy and radiation therapy (47, 48). It is also possible that voxtalisib affects pyruvate metabolism via MAPK signaling or via MYC, either downstream of the PI3K pathway or via non-specific drug effects (49, 50). Nonetheless, we did find that in the GS-2 model voxtalisib treatment leads to lower phospho-S6 levels, reduced HIF-1 activity (evidenced by lower CA-IX) and lower expression of LDH-A. This data confirms reduced PI3K signaling, and provides a mechanistic link between reduced signaling and our metabolic observations. Our findings are also identical to previous observations in GBM, breast and prostate cancer models (32, 33, 41). Similarly, we observed an increase in phospho-Chk1 in TMZ-treated tumors, linking the molecular effect of TMZ with the lower level of hyperpolarized lactate production, as previously observed in GBM (34, 35).

The metabolic effects observed in our hyperpolarized ^{13}C MRS study were detected within ~9 days of treatment in the case of the GS-2 model, and within ~6 days of treatment in the case of the U87-MG model, time points at which changes in tumor size were generally not detectable by MRI. As such, our data is consistent with previous studies showing that hyperpolarized Lac/Pyr can serve as an early indicator of drug-target engagement, and demonstrate that the hyperpolarized ^{13}C approach can also be used to monitor the effect of voxtalisib, possibly other dual PI3K/mTOR inhibitors, and combination therapy with TMZ. Our studies also show that reduced Lac/Pyr is associated with enhanced survival following treatment, independent of tumor size. Indeed, although in most cases treatment eventually affected tumor growth, in the case of GS-2 tumors voxtalisib did not lead to a detectable change in tumor size. Nonetheless, voxtalisib-treated mice lived statistically significantly longer than controls.

The recently completed first-in-man imaging study demonstrated the safety of hyperpolarized [1-^{13}C]-pyruvate as an agent for noninvasive characterization of metabolism in patients, and demonstrated the value of the hyperpolarized methodology for clinical studies (36). The approach used in our study could therefore be implemented in the clinic to aid in monitoring drug action and assessing likely response to PI3K pathway inhibitors. Such a noninvasive imaging approach would assist the treatment decision-making process at an early time point allowing for the advancement of precision medicine that is tailored to the individual patient.

Supplementary Material

Refer to Web version on PubMed Central for supplementary material.

Acknowledgments

The authors acknowledge M. VanCriekinge, S. Subramaniam, J. Crane, B. Olson, A. Elkhaled and R. Bok for their technical support, help with SIVIC and animal handling, as well as support from the hyperpolarized MRI Technology Resource Center (P41EB013598 D. B. Vigneron).

Funding: National Institute of Health R01CA154915 (S.M. Ronen)

References

1. Ostrom QT, Gittleman H, Liao P, Rouse C, Chen Y, Dowling J, et al. CBTRUS Statistical Report: Primary Brain and Central Nervous System Tumors Diagnosed in the United States in 2006–2010. Neuro-Oncology. 2013:15.
2. Stupp R, Mason WP, van den Bent MJ. Radiotherapy plus concomitant and adjuvant temozolomide for glioblastoma. N Engl J Med. 2005; 352:987–996. [PubMed: 15758009]
3. Sengupta S, Marrinan J, Frishman C, Sampath P. Impact of temozolomide on immune response during malignant glioma chemotherapy. Clin Dev Immunol. 2012:2012.
4. Johannessen TC, Bjerkvig R. Molecular mechanisms of temozolomide resistance in glioblastoma multiforme. Expert Rev Anticancer Ther. 2012; 12:635–642. [PubMed: 22594898]
5. Stupp R, Hegi ME, Mason WP, van den Bent MJ, Taphoornd MJB, Janzer RC, et al. Effects of radiotherapy with concomitant and adjuvant temozolomide versus radiotherapy alone on survival in glioblastoma in a randomised phase III study: 5-year analysis of the EORTC-NCIC trial. The Lancet Oncology. 2009; 10:459–466. [PubMed: 19269895]
6. Kesari S. Understanding glioblastoma tumor biology: the potential to improve current diagnosis and treatments. Semin Oncol. 2011:38.
7. Park CK, Lee SH, Kim TM, Choi SH, Park SH, Heo DS, et al. The value of temozolomide in combination with radiotherapy during standard treatment for newly diagnosed glioblastoma. J Neurooncol. 2013; 112:277–283. [PubMed: 23377829]
8. Network TCGATR. Comprehensive genomic characterization defines human glioblastoma genes and core pathways. Nature. 2008; 455:1061–1068. [PubMed: 18772890]
9. https://clinicaltrials.gov
10. Rodon J, Dienstmann R, Serra V, Tabernero J. Development of PI3K inhibitors: lessons learned from early clinical trials. Nat Rev Clin Oncol. 2013; 10:143–153. [PubMed: 23400000]
11. Ma DJ, Galanis E, Anderson SK, Schiff D, Kaufmann TJ, Peller PJ, et al. A phase II trial of everolimus, temozolomide, and radiotherapy in patients with newly diagnosed glioblastoma: NCCTG N057K. Neuro Oncol. 2014
12. Lassen U, Sorensen M, Gaziel TB, Hasselbalch B, Poulsen HS. Phase II study of bevacizumab and temsirolimus combination therapy for recurrent glioblastoma multiforme. Anticancer Res. 2013; 33:1657–1660. [PubMed: 23564811]

13. Kuger S, Graus D, Brendtke R, Günther N, Katzer A, Lutyj P, et al. Radiosensitization of Glioblastoma Cell Lines by the Dual PI3K and mTOR Inhibitor NVP-BEZ235 Depends on Drug-Irradiation Schedule. Transl Oncol. 2013; 6:169–179. [PubMed: 23544169]
14. Fan QW, Knight ZA, Goldenberg DD, Yu WEMK, Stokoe D, et al. A dual PI3 kinase/mTOR inhibitor reveals emergent efficacy in glioma. Cancer Cell. 2006; 9:341–349. [PubMed: 16697955]
15. Yu P, Laird AD, Du X, Wu J, Won KA, Yamaguchi K, et al. Characterization of the activity of the PI3K/mTOR inhibitor XL765 (SAR245409) in tumor models with diverse genetic alterations affecting the PI3K pathway. Mol Cancer Ther. 2014; 13:1078–1091. [PubMed: 24634413]
16. Papadopoulos KP, Tabernero J, Markman B, Patnaik A, Tolcher AW, Baselga J, et al. Phase I safety, pharmacokinetic, and pharmacodynamic study of SAR245409 (XL765), a novel, orally administered PI3K/mTOR inhibitor in patients with advanced solid tumors. Clin Cancer Res. 2014; 20:2445–2456. [PubMed: 24583798]
17. Salphati L, Heffron TP, Alicke B, Nishimura M, Barck K, Carano RA, et al. Targeting the PI3K pathway in the brain--efficacy of a PI3K inhibitor optimized to cross the blood-brain barrier. Clin Cancer Res. 2012; 18:6239–6248. [PubMed: 22992516]
18. Wan X, Harkavy B, Shen N, Grohar P, Helman LJ. Rapamycin induces feedback activation of Akt signaling through an IGF-1R–dependent mechanism. Oncogene. 2007:26.
19. Figlin RA, Kaufmann IJB. Targeting PI3K and mTORC2 in metastatic renal cell carcinoma: New strategies for overcoming resistance to VEGFR and mTORC1 inhibitors. Int J Cancer. 2013; 133:788–796. [PubMed: 23319457]
20. Chinot OL, Macdonald DR, Abrey LE, Zahlmann G, Kerloëguen Y, Cloughesy TF. Response assessment criteria for glioblastoma: practical adaptation and implementation in clinical trials of antiangiogenic therapy. Curr Neurol Neurosci Rep. 2013; 13:347. [PubMed: 23529375]
21. Courtney KD, Corcoran RB, Engelman JA. The PI3K Pathway As Drug Target in Human Cancer. J Clin Oncol. 2010; 28:1075–1083. [PubMed: 20085938]
22. Majósa C, Julià-Sapéb M, Alonsoa J, Serrallongaa M, Aguileraa C, Acebesc JJ, et al. Brain Tumor Classification by Proton MR Spectroscopy: Comparison of Diagnostic Accuracy at Short and Long TE. Am J Neuroradiol. 2004; 25:1696–1704. [PubMed: 15569733]
23. Zhang H, Ma L, Wang Q, Zheng X, Wu C, Xu BN. Role of magnetic resonance spectroscopy for the differentiation of recurrent glioma from radiation necrosis: a systematic review and meta-analysis. Eur J Radiol. 2014; 83:2181–2189. [PubMed: 25452098]
24. Nelson SJ. Multivoxel Magnetic Resonance Spectroscopy of Brain Tumors. Mol Cancer Ther. 2003; 2:497. [PubMed: 12748312]
25. Glunde K, Bhujwalla ZM, Ronen SM. Choline metabolism in malignant transformation. Nat Rev Cancer. 2011; 11:835–848. [PubMed: 22089420]
26. Venkatesh HS, Chaumeil MM, Ward CS, Haas-Kogan DA, James CD, Ronen SM. Reduced phosphocholine and hyperpolarized lactate provide magnetic resonance biomarkers of PI3K/Akt/mTOR inhibition in glioblastoma. Neuro Oncol. 2012; 14:315–325. [PubMed: 22156546]
27. Beloueche-Babari M, Jackson LE, Al-Saffar NM, Eccles SA, Raynaud FI, Workman P, et al. Identification of magnetic resonance detectable metabolic changes associated with inhibition of phosphoinositide 3-kinase signaling in human breast cancer cells. Mol Cancer Ther. 2006; 5:187–196. [PubMed: 16432178]
28. Koul D, Shen R, Kim YW, Kondo Y, Lu Y, Bankson J, et al. Cellular and in vivo activity of a novel PI3K inhibitor, PX-866, against human glioblastoma. Neuro Oncol. 2010; 12:559–569. [PubMed: 20156803]
29. Ardenkjaer-Larsen JH, Fridlund B, Gram A, Hansson G, Hansson L, Lerche MH, et al. Increase in signal-to-noise ratio of > 10,000 times in liquid-state NMR. Proceedings of the National Academy of Sciences of the United States of America. 2003; 100:10158–10163. [PubMed: 12930897]
30. Kurhanewicz J, Vigneron DB, Brindle K, Chekmenev EY, Comment A, Cunningham CH, et al. Analysis of Cancer Metabolism by Imaging Hyperpolarized Nuclei: Prospects for Translation to Clinical Research. Neoplasia. 2011; 13:81–97. [PubMed: 21403835]
31. Brindle K. Watching tumours gasp and die with MRI: the promise of hyperpolarised 13C MR spectroscopic imaging. Br J Radiol. 2012; 85:697–708. [PubMed: 22496072]

32. Chaumeil MM, Ozawa T, Park I, Scott K, James CD, Nelson SJ, et al. Hyperpolarized 13C MR spectroscopic imaging can be used to monitor Everolimus treatment in vivo in an orthotopic rodent model of glioblastoma. Neuroimage. 2012; 59:193–201. [PubMed: 21807103]
33. Ward CS, Venkatesh HS, Chaumeil MM, Brandes AH, Vancriekinge M, Dafni H, et al. Noninvasive detection of target modulation following phosphatidylinositol 3-kinase inhibition using hyperpolarized 13C magnetic resonance spectroscopy. Cancer Res. 2010; 70:1296–1305. [PubMed: 20145128]
34. Park I, Bok R, Ozawa T, Phillips JJ, James CD, Vigneron DB, et al. Detection of early response to temozolomide treatment in brain tumors using hyperpolarized 13C MR metabolic imaging. J Magn Reson Imaging. 2011; 33:1284–1290. [PubMed: 21590996]
35. Park I, Mukherjee J, Ito M, Chaumeil MM, Jalbert LE, Gaensler K, et al. Changes in Pyruvate Metabolism Detected by Magnetic Resonance Imaging Are Linked to DNA Damage and Serve as a Sensor of Temozolomide Response in Glioblastoma Cells. Cancer Res. 2014
36. Nelson SJ, Kurhanewicz J, Vigneron DB, Larson PEZ, Harzstark AJ, Ferrone M, et al. Metabolic Imaging of Patients with Prostate Cancer Using Hyperpolarized [1-13C]Pyruvate. Science Translational Medicine. 2013; 5:198.
37. Nelson SJ. Analysis of volume MRI and MR spectroscopic imaging data for the evaluation of patients with brain tumors. Magn Reson Med. 2001; 46:228–239. [PubMed: 11477625]
38. Crane JC, Olson MP, Nelson SJ. SIVIC: Open-Source, Standards-Based Software for DICOM MR Spectroscopy Workflows. Int J Biomed Imaging. 2013
39. jMRUI. http://www.mrui.uab.es/mrui/mrui_Overview.shtml
40. Mnova. http://mestrelab.com/
41. Dafni H, Larson PE, Hu S, Yoshihara HA, Ward CS, Venkatesh HS, et al. Hyperpolarized 13C spectroscopic imaging informs on hypoxia-inducible factor-1 and myc activity downstream of platelet-derived growth factor receptor. Cancer Res. 2010; 70:7400–7410. [PubMed: 20858719]
42. Mason WP, Macneil M, Kavan P, Easaw J, Macdonald D, Thiessen B, et al. A phase I study of temozolomide and everolimus (RAD001) in patients with newly diagnosed and progressive glioblastoma either receiving or not receiving enzyme-inducing anticonvulsants: an NCIC CTG study. Invest New Drugs. 2012; 30:2344–2351. [PubMed: 22160854]
43. Prasad G, Sottero T, Yang X, Mueller S, James CD, Weiss WA, et al. Inhibition of PI3K/mTOR pathways in glioblastoma and implications for combination therapy with temozolomide. Neuro Oncol. 2011; 13:384–392. [PubMed: 21317208]
44. Esmaeili M, Bathen TF, Engebråten O, Mælandsmo GM, Gribbestad IS, Moestue SA. Quantitative (31)P HR-MAS MR spectroscopy for detection of response to PI3K/mTOR inhibition in breast cancer xenografts. Magn Reson Med. 2014; 71:1973–1981. [PubMed: 23878023]
45. Al-Saffar NM, Marshall LV, Jackson LE, Balarajah G, Eykyn TR, Agliano A, et al. Lactate and choline metabolites detected in vitro by nuclear magnetic resonance spectroscopy are potential metabolic biomarkers for PI3K inhibition in pediatric glioblastoma. PLoS One. 2014:9.
46. Al-Saffar NM, Jackson LE, Raynaud FI, Clarke PA, Ramírez de Molina A, Lacal JC, et al. The phosphoinositide 3-kinase inhibitor PI-103 downregulates choline kinase alpha leading to phosphocholine and total choline decrease detected by magnetic resonance spectroscopy. Cancer Res. 2010; 70:5507–5517. [PubMed: 20551061]
47. Sandulache VC, Chen Y, Skinner HD, Lu T, Feng L, Court LE, et al. Acute Tumor Lactate Perturbations as a Biomarker of Genotoxic Stress: Development of a Biochemical Model. Mol Cancer Ther. 2015; 14:2901–2908. [PubMed: 26376962]
48. Lin G, Andrejeva G, Wong Te Fong AC, Hill DK, Orton MR, Parkes HG, et al. Reduced Warburg effect in cancer cells undergoing autophagy: steady- state 1H–MRS and real-time hyperpolarized 13C–MRS studies. PLoS One. 2014; 9:e9264.
49. Lodi A, Woods SMMRS. Treatment with the MEK inhibitor U0126 induces decreased hyperpolarized pyruvate to lactate conversion in breast but not in prostate cancer cells. NMR Biomed. 2013; 26:299–306. [PubMed: 22945392]
50. Wu SH, Bi JF, Cloughesy T, Cavenee WK, Mischel PS. Emerging function of mTORC2 as a core regulator in glioblastoma: metabolic reprogramming and drug resistance. Cancer Biol Med. 2014; 11:255–263. [PubMed: 25610711]

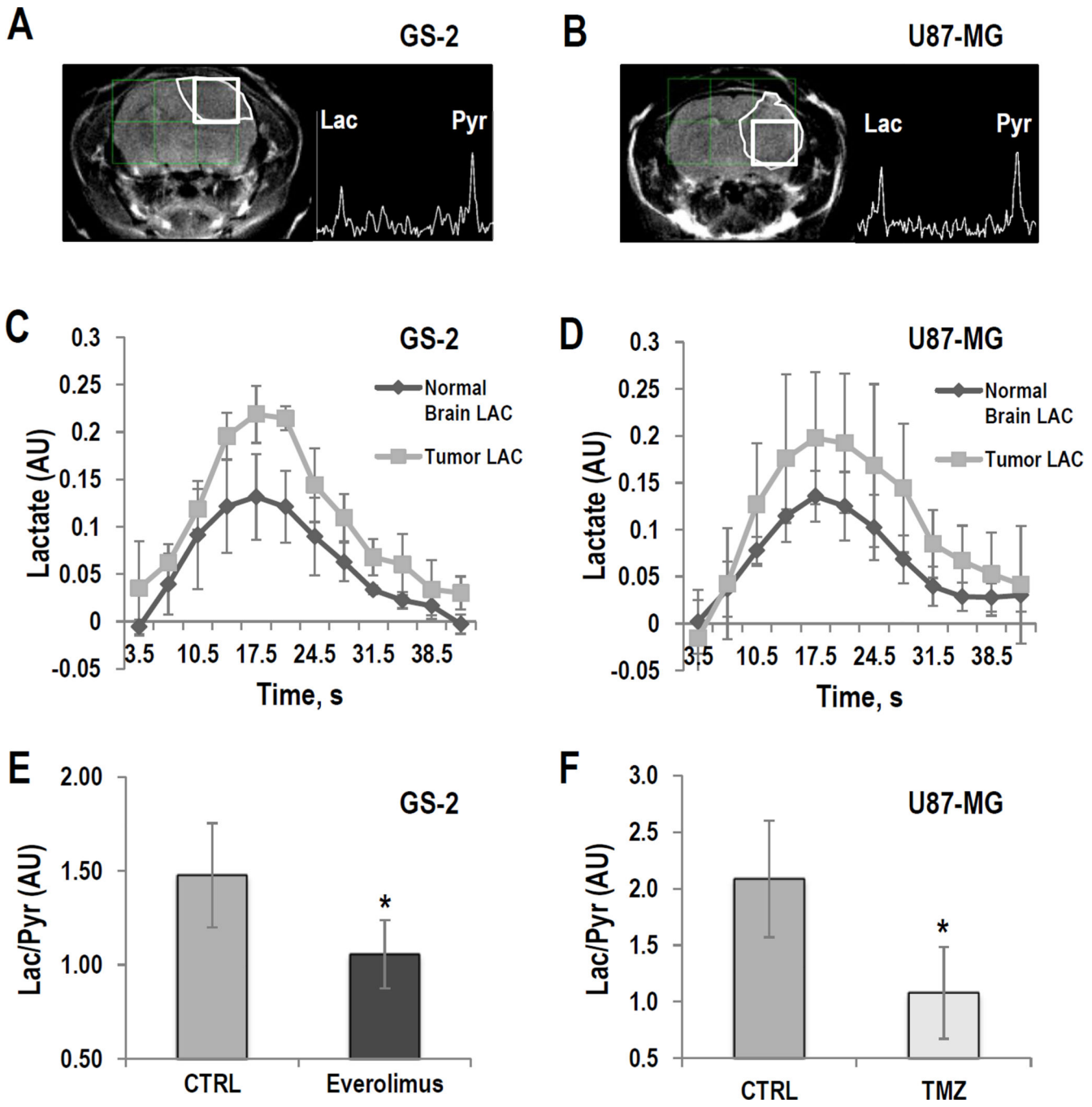

Figure 1.

GS-2 (left) and U87-MG models (right): (A and B) T2-weighted images and corresponding hyperpolarized ^{13}C MR spectra from tumor voxels. (C and D) Temporal evolution of hyperpolarized [1-^{13}C]-lactate in the tumor and in normal brain voxels. (E and F) Average hyperpolarized Lac/Pyr detected in tumor voxel in GS-2 tumors treated with Everolimus at D9±2 and in U87-MG tumors treated with TMZ at D6±1. *: $P<0.05$

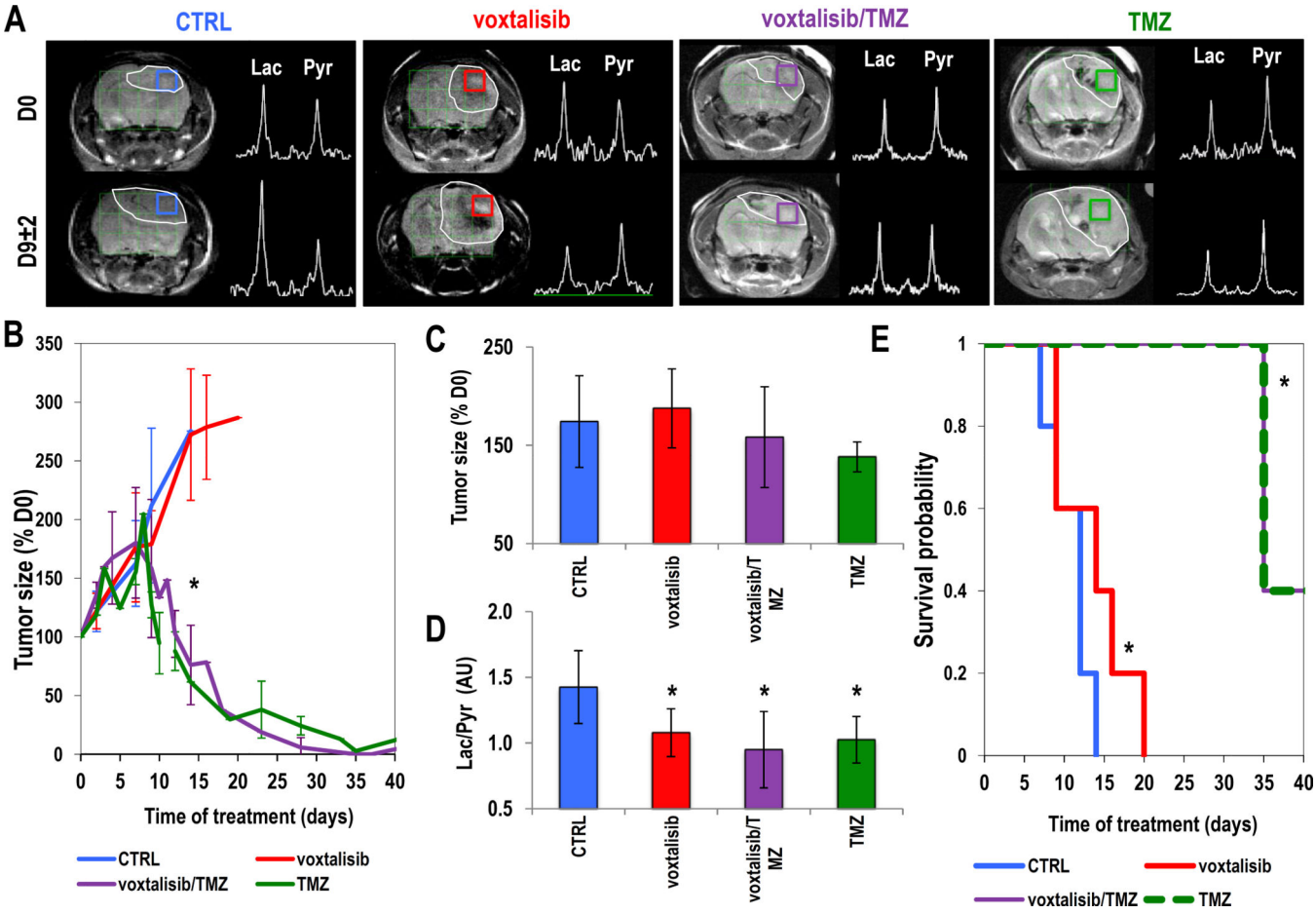

Figure 2.

GS-2 model: (A) Axial T2-weighted images and corresponding hyperpolarized ^{13}C MRSI spectra from the tumor voxel at D0 (top) and D9±2 of treatment (bottom). The tumor regions are contoured with white dashed line. (B) Temporal evolution of average tumor size as a percentage of pre-treatment value. (C) Average tumor size detected at D9±2. (D) Average Lac/Pyr detected at D9±2. (E) Kaplan-Meier survival curves comparing control and treatment groups. *: $P<0.05$

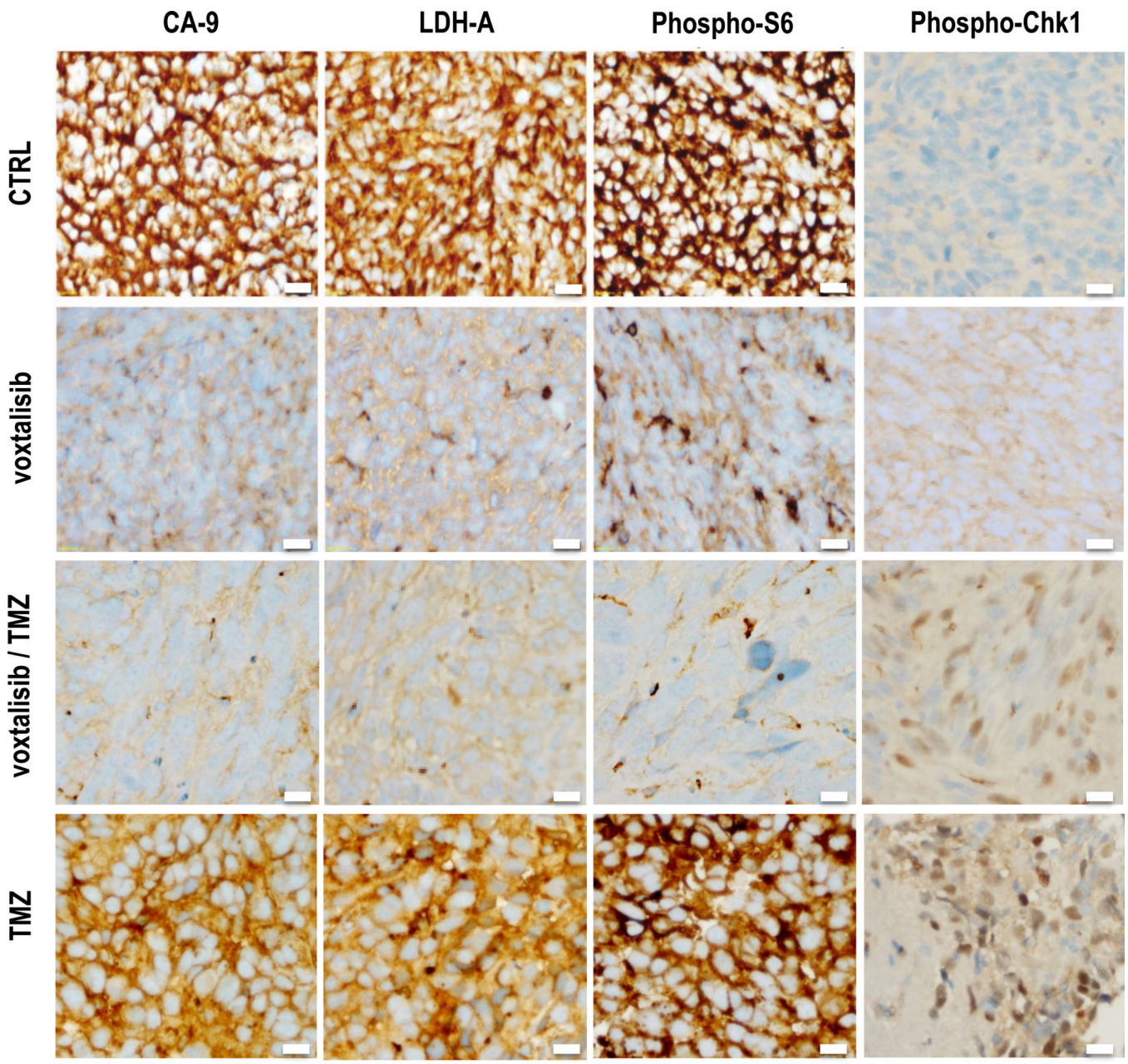

Figure 3.

GS-2 model: IHC showing the expression of CA-IX, LDH-A, phospho-S6 and phospho-Chk1 for each treatment group at the end of study. Bar indicates 20μm.

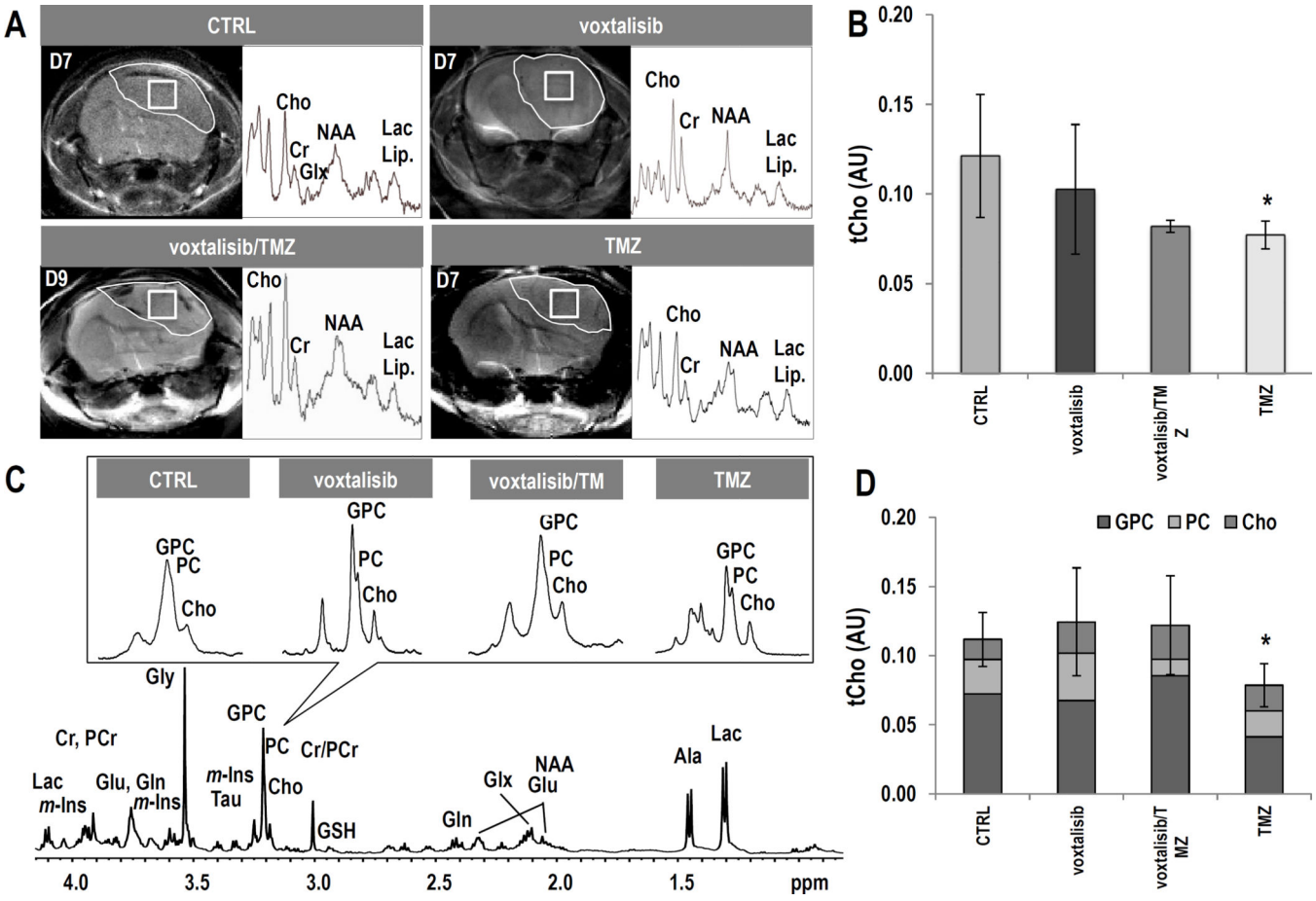

Figure 4.

GS-2 model: (A) Axial T2-weighted images and corresponding ^{1}H spectra of the tumor voxel from each treatment group. (B) Average tCho levels at D9±2. (C) Representative *ex vivo* ^{1}H HR-MAS spectrum of a biopsy from control tumor. The inserts, zoomed on choline-containing metabolites, illustrate each treatment group. (D) Comparison of tCho levels and individual choline-containing metabolites. Error bars correspond to the standard deviation of tCho.

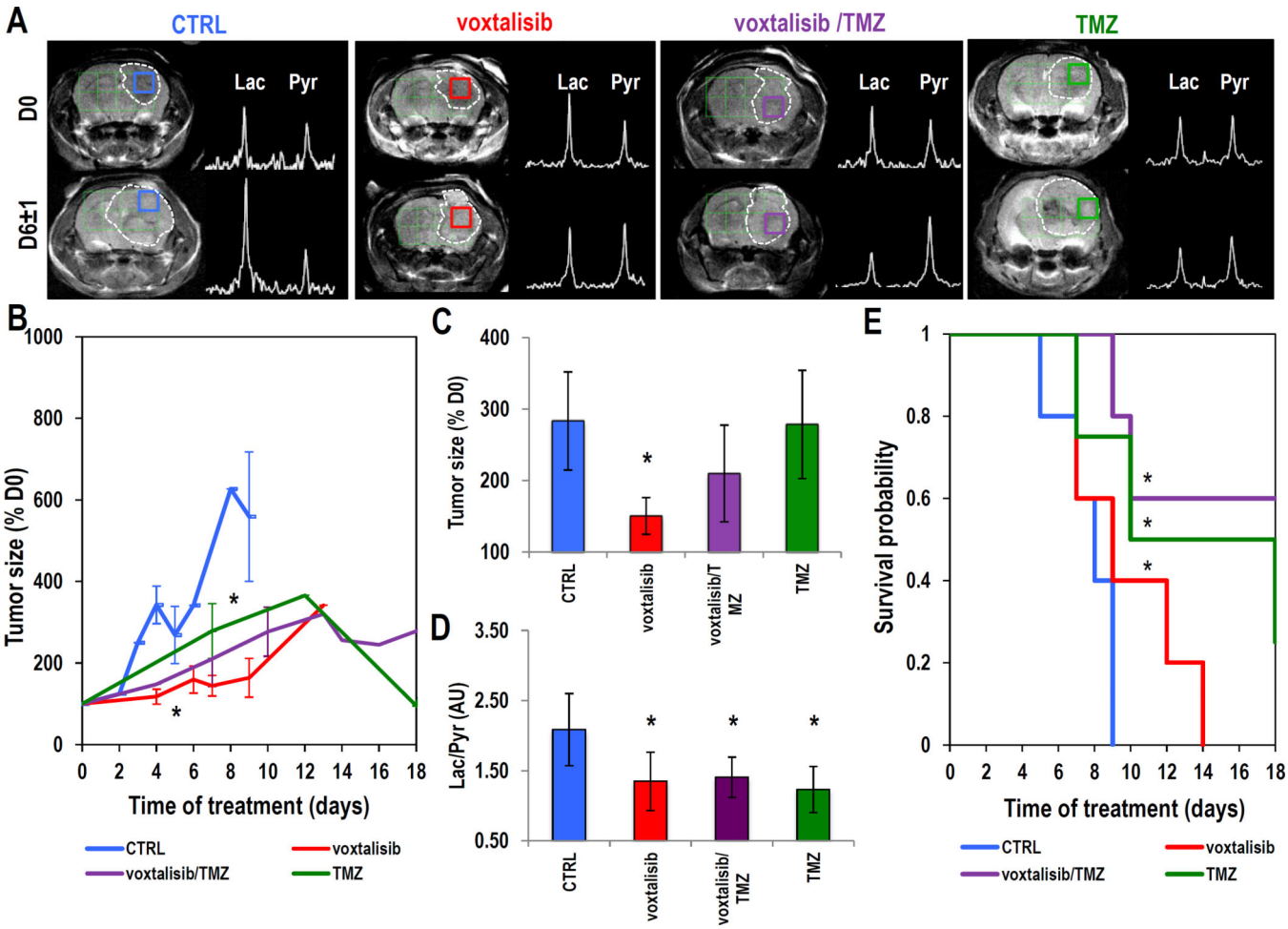

Figure 5.

U87-MG model: (A) Anatomical axial T2-weighted images and corresponding hyperpolarized ^{13}C MRSI spectra from the tumor voxel at D0 (top) and D6±1 of treatment (bottom). Tumor regions are contoured in white dashed line. (B) Temporal evolution of average tumor size. (C) Average tumor size detected at D6±1 of treatment. (D) Average hyperpolarized Lac/Pyr detected at D6±1 of treatment. (E) Kaplan-Meier survival curves comparing survival between control and treatment groups.

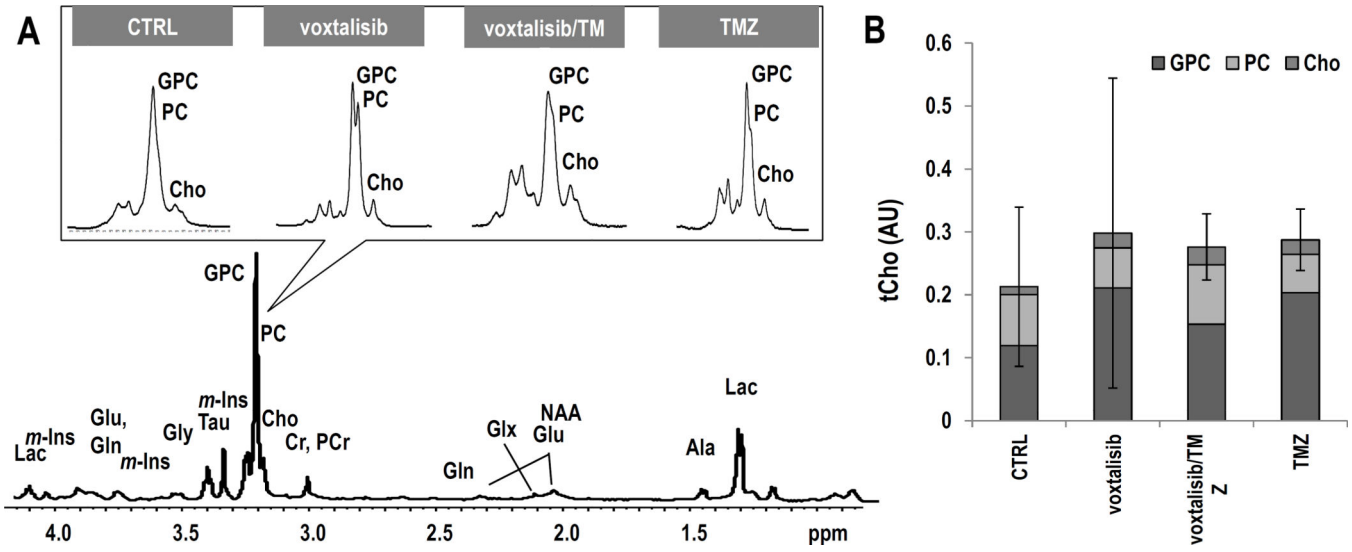

Figure 6.

U87-MG tumor model: (A) Representative *ex vivo* ^{1}H HR-MAS spectra from of a biopsy of control tumor. Inserts exhibit spectra zoomed on the choline region. (B) tCho levels and individual choline-containing metabolites. The error bars correspond to the standard deviation of the tCho.